Examples of the potential of DNS for the understanding of reactive multiphase flows.

Julien Reveillon, Cécile Péra, Zakaria Bouali

EXAMPLES OF THE POTENTIAL OF DNS FOR THE UNDERSTANDING OF REACTIVE MULTIPHASE FLOWS

J. Reveillon*, C. Pera†, Z. Bouali*,†
*CORIA, University of Rouen,
avenue de l'Université BP12, 76801 Saint Etienne du Rouvray, France
e-mail: Julien.Reveillon@coria.fr

† IFP, 1 et 4 avenue de Bois-Préau, 92852 Rueil Malmaison Cedex, France

May 7, 2010

1 ABSTRACT

The objective of this article is to point out the ability of the multiphase flow DNS (Direct Numerical Simulation) to help to understand basic physics and to interpret some experimental observations. To illustrate the DNS potential to give access to key phenomena involved in reactive multiphase flows, several recent results obtained by the authors are summed up with a bridge to experimental results. It includes droplet dispersion, laminar spray flame instability, spray combustion regimes or acoustic modulation effect on a two-phase flow Bunsen burner. As a perspective, two-phase flow DNS auto-ignition is considered thanks to a skeletal mechanism for the n-heptane chemistry involving 29 species and 52 reactions. Results highlight evaporating droplet effects on the auto-ignition process that is generally dramatically modified by spray distribution resulting from the turbulent fluid motion. This paper shows that DNS is a powerful tool to understand the intricate coupling between the evaporating spray, the turbulent fluid motion and the detailed chemistry, inseparable in the experimental context.

2 INTRODUCTION

From liquid jet atomization down to droplet evaporation and vapor combustion, two-phase flows are commonly encountered in many industrial devices such as engines or furnaces. Both from the economical and the ecological point of views, it is nowadays of primary importance to ensure low fuel consumption for vehicles, while maintaining minimal pollutant emissions. Numerical modeling of the phenomena in the combustion chamber is today a necessary stage when developing or improving engines. Model development is

based on the understanding of the basic physical phenomena. For this purpose, experimental measurements may be of a great help but most often they only bring partial information. Indeed, the simultaneous presence of a turbulent flow, an evaporating spray and a combustion process in a confined geometry limits the capability of experimental techniques. On the other hand, direct numerical simulations (DNS) of the flow offer essential information although such simulations have severe limitations that will be detailed in the following. Therefore, an ideal research project would be to simultaneously carry out numerical and experimental studies on some basic configurations to understand all the underlying phenomena, especially for two-phase flow turbulent combustion.

A DNS consists in resolving, with accurate numerical methods, the full set of partial differential equations describing the physics of the problem. Despite claiming for the resolution of the whole physics, these equations often result from a closure at a given level of the physics. Navier-Stokes equations or Fick's law in scalar transport equations are themselves models issued from the analysis of the motion of the various molecules of the flow. However, as far as low or medium range Mach number flow are considered, Navier-Stokes equations are considered to be an exact representation of reality. Providing that ideal conditions are met (simple geometry, high order - non dissipative numerical schemes, grid adapted to all the characteristic scales of the flow, ...), DNS offers a unique description of the physical phenomena with a direct access to all the flow parameters. However, considering two-phase flows, good intentions have to face reality: the presence of an interface between gas and liquid leads to characteristic scales and gradients far too extreme to be resolved without the sacrifice of accuracy. Considering the present day supercomputer capabilities, considered as weak from a DNS point of view, the most frequent alternative is the introduction of some Lagrangian models [1, 2, 3] to account for the spray. This leads to DNS-DPS (Discrete Particle Simulation), results of which are correct enough to help us to understand many physical phenomena.

DNS was first introduced 35 years ago by Orzag and Patterson [4] and then Rogallo [5] and Lee *et al.* [6] for the simulation of inert gaseous flows. It has been used in a large range of applications since. During the last two decades, DNS of reactive flows have been carried out to study non-premixed, partially premixed and premixed turbulent combustion of purely gaseous conditions [7, 8, 9, 10, 11]. DNS has been extended to two-phase flows since the pioneering work of Riley and Patterson [12]. Most of the first numerical studies were dedicated to solid particle dispersion (see, for instance, references [13, 14, 15, 16, 17]). More recently, Mashayek *et al.* [18], Reveillon *et al.* [19] and Miller and Bellan [2] have conducted the first DNS with evaporating droplets in turbulent flows. Since then, DNS of two-phase flows have been extended to incorporate two-way coupling effects, multicomponent fuels, ... but also to deal with spray evaporation and combustion phenomena [1, 2, 3, 20, 21]. At the same time, combustion kinetics has been extended from simple single-step chemistry [3] to skeletal mechanism [22, 23, 24] giving clues for the understanding of real complex configurations involving intricate coupling between evaporating droplets, turbulent fluid motion and combustion.

Even if DNS offers all elementary components (turbulence, droplets, combustion), direct comparisons between reactive multiphase flow DNS and experiments still raise numerous problems and have some limitations. Nevertheless, DNS is nowadays a powerful tool that can be used to help in the interpretation of experimental observations. The ob-

jective of the present paper is to illustrate the potential of the DNS for the understanding of the basic physics involved in reactive multiphase flows and for the interpretation of experimental observations. After a brief presentation of the numerical procedures, some examples demonstrate the capability of DNS to help to understand the complex correlations between spray, turbulence and combustion. It includes droplet dispersion, laminar spray flame instability, spray combustion regimes and acoustic modulation effect on a two-phase flow Bunsen burner. Eventually, two-phase flow DNS auto-ignition is considered through a skeletal mechanism. Results point out the influence of the evaporating spray on the auto-ignition process that dramatically depends on droplet segregation resulting from the turbulent mixing.

3 DNS-DPS OF TWO-PHASE FLOWS

In the present paper, DNS-DPS is considered in the framework of gas-liquid flows. Even if models have to be introduced, DNS-DPS of spray dispersion, evaporation and combustion may offer information that could not be obtained otherwise. The objective is to optimize the modeling of the interactions between both phases well enough to capture and to understand the prevalent physical phenomena and to develop models for LES (Large Eddy Simulation) and RANS (Reynolds Averaged Navier-Stokes) simulations.

In combustion chambers, the liquid is generally directly injected before being atomized. A polydispersed spray emerges from the breakup of the liquid core. The turbulent dispersion of the evaporating droplets directly leads to a fuel/oxidizer mixture. The accurate modeling of the combustion regimes depends on a correct estimation of all the above mentioned processes. DNS-DPS tries to consider all of them. However, it is not possible to do it at once because physics and characteristic scales involved in atomization (with the presence of an interface) are too singular and need specific models and numerical methods. It is not the purpose of the present paper to detail such models and methods. However, a brief example of a DNS detailing the atomization of a liquid jet is first demonstrated before the description of the Eulerian/Lagrangian coupling generally used in DNS-DPS of polydispersed sprays.

3.1 Interface resolving methods

Both gas and liquid are described by the Navier-Stokes equations. When both phases are simultaneously considered, the presence of an interface, localizing the sudden modification of the flow properties, cannot be captured by single-phase solvers. Specific numerical methods have thus to be used to describe the time and space evolution of this interface.

The interface tracking F is done by solving the following equation:

$$\frac{\partial F}{\partial t} + U_i \frac{\partial F}{\partial x_i} = 0 \tag{1}$$

where U_i is the flow velocity at the interface position. Several works [25, 26, 27] have been dedicated to the direct resolution of such an equation leading to a 'DNS' of a liquid/gas interface (Fig. 1).

Figure 1: DNS of the atomization of a liquid jet [27].

Two procedures are generally used to describe the evolution of an interface: the level-set (LS) method and the volume of fluid (VOF) method. In the first case, the interface is represented by a zero level line of the function F. This function gives the distance to the interface of any point of the grid. If Γ is the interface, it is defined by $\Gamma = \{\vec{x}|F(\vec{x},t) = 0\}$. On the other hand, the VOF method uses the phase function F_k to define the volume occupied by each phase k in a cell. A unitary value of F_k corresponds to a cell completely filled with the k phase and a null value indicates the absence of this phase in the cell. Both methods are complementary. LS offers a direct description of the shape of the interface but has difficulties to conserve mass. On the other hand, VOF method is mass conservative but interface reconstruction is not straightforward. Consequently, the actual trend is to couple both procedures [27] in order to ease the interface tracking.

If liquid atomization may be characterized with specific models describing the interface, supercomputer capabilities are not large enough to describe the atomization process along with dispersion, evaporation and combustion. Therefore another family of DNS solvers (DNS-DPS) is generally used to simulate the evolution of a polydispersed evaporating spray. The following sections describe the corresponding physical models and the various difficulties.

3.2 Carrier phase description

The carrier phase is a compressible Newtonian fluid following the equation of state for a perfect gas. The instantaneous balance equations describe the evolution of mass ρ, momentum $\rho\mathbf{U}$, total (except chemical) energy E_t and species mass fraction. Y_F denotes the mass fraction of gaseous fuel resulting from spray evaporation and Y_m stands for all other species. The following set of balance equations are solved where usual notations are

adopted:

$$\frac{\partial \rho}{\partial t} + \frac{\partial \rho U_l}{\partial x_l} = \dot{m} \tag{2}$$

$$\frac{\partial \rho U_i}{\partial t} + \frac{\partial \rho U_i U_l}{\partial x_l} = -\frac{\partial P}{\partial x_i} + \frac{\partial \sigma_{il}}{\partial x_l} + \dot{v}_i \tag{3}$$

$$\frac{\partial \rho E_t}{\partial t} + \frac{\partial (\rho E_t + P) U_l}{\partial x_l} = \frac{\partial}{\partial x_l}\left(\lambda \frac{\partial T}{\partial x_l}\right) + \frac{\partial \sigma_{il} U_l}{\partial x_i} + \rho \dot{\omega}_e + \dot{e} \tag{4}$$

$$\frac{\partial \rho Y_F}{\partial t} + \frac{\partial \rho Y_F U_l}{\partial x_l} = \frac{\partial}{\partial x_l}\left(\rho D_F \frac{\partial Y_F}{\partial x_l}\right) + \rho \dot{\omega}_F + \dot{m} \tag{5}$$

$$\frac{\partial \rho Y_m}{\partial t} + \frac{\partial \rho Y_m U_l}{\partial x_l} = \frac{\partial}{\partial x_l}\left(\rho D_m \frac{\partial Y_m}{\partial x_l}\right) + \rho \dot{\omega}_m \tag{6}$$

with

$$\sigma_{ij} = \mu\left(\frac{\partial U_i}{\partial x_j} + \frac{\partial U_j}{\partial x_i}\right) - \frac{2}{3}\mu \frac{\partial U_l}{\partial x_l}\delta_{ij}$$

together with the equation of state for perfect gases:

$$P = \rho R T$$

where R is the ratio of the perfect gas constant with the carrier phase molar mass.

Various source terms are present: $\dot{\omega}_F$, $\dot{\omega}_m$ and $\dot{\omega}_e$ terms are related to the chemical reaction processes whereas $\dot{m}$, $\dot{\mathbf{v}}$, $\dot{e}$ result from a two-way coupling between the carrier phase and the spray. These terms will be detailed in a following section.

The sixth order Padé scheme from Lele [28] has been used to compute spatial derivative of the gas phase transport equations on a regular mesh. The time integration of both spray and gas phase equations is carried out with a third order explicit Runge-Kutta scheme with a minimal data storage method [29]. A third order interpolation is used when gaseous phase properties must be determined at the droplet positions.

3.3 Dispersed phase Lagrangian description

As described by Reeks [30], it is possible to take into account many forces to characterize the droplet dynamics. However, the purpose of this text is to present a basis to carry out DNS-DPS of two-phase flows. Thus, because of the high density ratio between liquid and gas phases, the drag force, which is prevalent, has only been selected. Additionally, several usual assumptions have been used: some of them are given in the following, others may be found in Sirignano reference paper [31]. First, the spray is supposed dispersed and each droplet is unaware of the existence of the others. Any internal liquid circulation or droplet rotation is neglected and an infinite liquid heat conduction coefficient is assumed. As a consequence, liquid core temperature remains uniform but evolves as a function of time. The spray is supposed to be local sources of mass following the saturation law and modifying momentum and gaseous fuel topology, depending on the local gas temperature, pressure and vapor mass fraction.

3.3.1 Position and velocity

By denoting $\mathbf{V}_k$ and $\mathbf{X}_k$ the velocity and position vectors of droplet k, respectively, the following relations:

$$\frac{d\mathbf{V}_k}{dt} = \frac{1}{\beta_k^{(V)}}\left(\mathbf{U}\left(\mathbf{X}_k,t\right)-\mathbf{V}_k\right) \tag{7}$$

$$\frac{d\mathbf{X}_k}{dt} = \mathbf{V}_k \tag{8}$$

are used to track any k droplet evolution throughout the computational domain. The vector $\mathbf{U}\left(\mathbf{X}_k,t\right)$ represents the gas velocity at the droplet position $\mathbf{X}_k$. The right hand side term of equation (7) stands for a drag force applied to the droplet and $\beta_k^{(V)}$ is a kinetic relaxation time. It may be obtained from the k^{th} droplet dynamics:

$$m_k\frac{d\mathbf{V}_k}{dt} = \mathbf{D}_k \tag{9}$$

where $\mathbf{D}_k$ is the drag force applied to the k^{th} droplet considered as a sphere. It directly leads to the kinetic relaxation time for the k^{th} droplet:

$$\beta_k^{(V)} = \frac{\rho_d a_k^2}{18 C_{uk}\mu} \tag{10}$$

where a_k is the droplet diameter, ρ_d is the liquid density and μ is the gas viscosity. $C_{uk} = 1 + Re_k^{2/3}/6$ is a corrective coefficient to account for the variation of the drag factor according to the droplet Reynolds number $Re_k = \rho \mid \mathbf{u}(\mathbf{x}_k - \mathbf{v}_k) \mid a_k/\mu$.

3.3.2 Heating and evaporation

The heating and evaporation of each droplet is described through a normalized quantity B_k, denominated the "mass transfer number". B_k is the normalized flux of gaseous fuel between the droplet surface and the surrounding gas. It may be written:

$$B_k = \frac{Y_{Fk}^s - Y_F(\mathbf{X}_k)}{1 - Y_{Fk}^s} \tag{11}$$

where Y_{Fk}^s is the gaseous fuel mass fraction at the droplet surface and $Y_F(\mathbf{X}_k)$ is the fuel mass fraction in the surrounding gas at the droplet position. By solving the mass and energy balance equations at the surface of a vaporizing droplet in a quiescent atmosphere [32], the following relations for the surface and the temperature evolution of each droplet k are found:

$$\frac{da_k^2}{dt} = -\frac{a_k^2}{\beta_k^{(a)}} \tag{12}$$

$$\frac{dT_k}{dt} = \frac{1}{\beta_k^{(T)}}\left(T(\mathbf{X}_d) - T_k - \frac{B_k L_v}{C_p}\right) \tag{13}$$

Again, characteristic relaxation times appear. They are defined by:

$$\beta_k^{(a)} = \frac{S_c}{4Sh_c}\frac{\rho_d}{\mu}\frac{a_k^2}{\ln(1+B_k)} \tag{14}$$

$$\beta_k^{(T)} = \frac{P_r}{6Nu_c}\frac{C_d}{C_p}\frac{\rho_d a_k^2}{\mu}\frac{B_k}{\ln(1+B_k)} \tag{15}$$

where normalized gas and liquid heat capacities are denoted C_p and C_d, respectively. As L_v, the latent heat of evaporation, C_p and C_d are constant in the present set of equations. Sc and Pr are the Schmidt and Prandtl numbers, respectively. Sh_c and Nu_c are the convective Sherwood and Nusselt numbers, respectively. They are both equal to 2 in a quiescent atmosphere, but a correction has to be applied in a convective environment. In this context, the empirical expressions from [32] are used.

One of the most accurate models to describe the evaporation process is to consider a phase equilibrium at the interface using the Clausius-Clapeyron relation:

$$\frac{d\ln(P_k^s)}{dT} \approx \frac{L_v}{R_F T^2} \tag{16}$$

where R_F is the specific gas constant of the gaseous fuel. It leads to the following expression for the partial pressure P_k^s of fuel vapor at the surface of the droplet:

$$P_k^s = P_{ref}\exp\left(-\frac{L_v}{R_F}\left(\frac{1}{T_k^s}-\frac{1}{T_{ref}}\right)\right) \tag{17}$$

where P_{ref} and T_{ref} are two reference parameters. T^s is the gas temperature at the droplet surface. Within each droplet, the temperature T_k is spatially uniform. Thus, it is equal to the temperature of the gas at the interface $T_k = T^s = T_k^s$.

The gaseous fuel mass fraction at the surface of the droplet is computed following:

$$Y_{Fk}^s = \left(1+\frac{W}{W_F}\left(\frac{P(\mathbf{X}_d)}{P_k^s}-1\right)\right)^{-1} \tag{18}$$

where W and W_F are the mixture and the fuel molar weights, respectively. Once the gaseous fuel mixture fraction at the droplet surface is known thank to relation (18), the varying number B_k is determined with equation (11). Consequently, equations (12) and (13), describing the evolution of droplet surface and temperature, are closed.

It is noteworthy that mass and heat transfer between the carrier phase and the droplets always consider the surrounding gas properties. However, as far as DNS-DPS is concerned, individual droplet combustion regime is not considered. Either droplets are evaporated before combustion takes place or group combustion, as defined by Chiu *et al.* [33], occurs.

3.4 Eulerian/Lagrangian coupling

The terms $\dot{m}$, $\dot{\mathbf{v}}$ and $\dot{e}$, in equations (2) to (5), are source terms for the gaseous phase mass, momentum and energy due to transfers from liquid phase, *i.e.* exchanges from the Lagrangian quantities to the Eulerian grid. Every Lagrangian source has to be distributed

over the Eulerian nodes by adding the volumic contributions from droplets. A particle-source-in-cell (PSI-cell) method [34] is generally used [35]. The mass, momentum and energy source terms are instantaneously distributed in the cells surrounding the considered droplets proportionally to the inverse of the distance between the cell and the droplet. Consequently, a weak numerical dispersion appears in the DNS-DPS framework. In real spray flows, this distribution is not instantaneous and further assumptions are needed to perform simulations. To address this issue, droplets can be resolved but this solution is limited to test cases with only a few droplets [36]. Another solution is to introduce a diffusion delay between the droplet and the surrounding nodes. However, in the case of reacting flows, some of the evaporated fuel would not directly interact with the local flames. Defining an alternative way remains an open task for the time being.

For each Eulerian node, a control volume $\mathcal{V}$ is defined based on the mid-distance with the neighboring nodes. If an isotropic Cartesian grid is considered ($\Delta = x_{i+1} - x_i = \Delta_x = \Delta_y = \Delta_z$), then $\mathcal{V} = \Delta^3$. The mass source term applied to any Eulerian node n is denoted $\dot{m}^{(n)}$:

$$\dot{m}^{(n)} = \frac{1}{\mathcal{V}} \sum_k -\alpha_k^{(n)} \frac{dm_k}{dt} \tag{19}$$

where $\sum_k$ is the sum over all the droplets affecting the node n. $\alpha_k^{(n)}$ is the distribution coefficient of the k^{th} droplet source term on the node n. Considering all the nodes affected by the k^{th} droplet, it is necessary to have $\sum_n \alpha_k^{(n)} = 1$ to conserve mass, momentum and energy during the Lagrangian/Eulerian coupling. In fact, $\alpha_k^{(n)}$ is the portion of the control volume of the node n intersecting the control volume of the k^{th} droplet:

$$\alpha_k^{(n)} = \frac{1}{\mathcal{V}} \prod_{i=1}^{3} \left(\Delta - \mid x_i^{(n)} - x_{ki} \mid \right) \tag{20}$$

where $x_i^{(n)}$ and x_{ki} are the coordinates along the i^{th} direction of the node n and the k^{th} droplet, respectively. This approach is generally used as far as dispersed particles are considered (see references [1, 37, 38, 39] and references therein).

The mass of the k^{th} droplet in the neighborhood of the node is $m_k = \rho_d \pi a_k^3/6$ and, using equations (12) and (19), one may write:

$$\dot{m}^{(n)} = \rho_d \frac{\pi}{4} \frac{1}{\mathcal{V}} \sum_k \alpha_k^{(n)} a_k^3 / \beta_k^{(a)} \tag{21}$$

Similarly, the following relation:

$$\dot{\mathbf{v}}^{(n)} = \frac{1}{\mathcal{V}} \sum_k -\alpha_k^{(n)} \frac{dm_k \mathbf{V}_k}{dt} \tag{22}$$

leads to the expression of the momentum source term:

$$\dot{\mathbf{v}}^{(n)} = -\rho_d \frac{\pi}{4} \frac{1}{\mathcal{V}} \sum_k \alpha_k^{(n)} a_k^3 \left(\frac{2}{3} \frac{\mathbf{U}(\mathbf{X}_d, t) - \mathbf{V}_k}{\beta_k^{(V)}} - \frac{\mathbf{V}_k}{\beta_k^{(a)}} \right) \tag{23}$$

The energy variation of the gaseous flow induced by the droplets inside the volume $\mathcal{V}$ may be written:

$$\dot{e}^{(n)} = \frac{1}{\mathcal{V}} \sum_k -\alpha_k^{(n)} \frac{dm_k C_d T_k}{dt} \tag{24}$$

and it may be developed as:

$$\dot{e}^{(n)} = -C_d \rho_d \frac{\pi}{4} \frac{1}{\mathcal{V}} \sum_k \alpha_k^{(n)} a_k^3 \left(\frac{2}{3} \frac{T(\mathbf{X}_d, t) - T_k - B_k L_v / C_p}{\beta_a^{(T)}} + \frac{T_k}{\beta_k^{(a)}} \right) \tag{25}$$

This last equation details how the energy provided to the droplet is distributed between evaporation and liquid core heating and how a part of this energy is lost due to liquid mass reduction.

From a general point of view, DNS-DPS simulations are accurate as far as the validity domain of the DNS and Lagrangian modeling are respected. It means that the turbulent Reynolds number remains small (generally between 30 and 150) and the geometry is simple enough to conserve high order numerical schemes. The dispersed phase must keep a mass loading ratio smaller than 0.1 and, to avoid numerical dispersion of the spray source terms, the droplets slip velocity reamins small. The CFL number is such that droplets are not able to cross more than half a cell during one time step. Because of the weak loading ratio, collisions as well as coalescence may be neglected and the droplets are too small to undergo a rupture.

3.5 Reaction rate

Detailed chemistry may be used to determine the chemical source terms $\dot{\omega}_e$, $\dot{\omega}_F$ and $\dot{\omega}_m$ appearing in the energy (Eq. (4)) and species balance equations (Eqs. (5) and (6)). Complete kinetics takes into account all reactions between all initial and final chemical species as well as their intermediates. For a simple hydrocarbon, it represents at least hundreds of reactions between dozens of chemical species. The chemistry solving computational cost is quite significant and results may be uncertain because it may be difficult to estimate some of the coefficients of the quickest reactions involving sparse species. Therefore, complex chemistry is not presently directly introduced and chemistry information is rather provided in the form of reduced kinetics by defining a reactional set of priorities. An alternative is to conserve all the information contained in the complex kinetics by solving it for various conditions defined by reference parameters (temperature, mixture fraction, main species mass fraction...) and storing the results in a database. Since detailed kinetics is time consuming, the additional computation of the evolution of millions of droplets is overly expansive in most cases which makes, today, the association DNS + Lagrangian solver + detailed kinetics a luxurious type of computation that is only seldom met [23]. Nevertheless, in order to study n-heptane auto-ignition process, a skeletal mechanism involving 29 species and 52 reactions [40] has been considered and the DNS-DPS code has been coupled with a solver dedicated to the computation of detailed chemistry. Solvers like Cantera [41] or Chemkin [42] are ideal candidates.

Detailed chemical kinetics is not inevitably required in combustion studies. Very often, one only needs to estimate the global impact of the presence of a flame within a flow

without knowing the reactional details. It is within this framework that a global reaction scheme can be used. In this case, chemical kinetics is reduced to a unique irreversible single-step reaction:

$$Fuel + Oxidizer \longrightarrow Products \tag{26}$$

If the reaction rate from Eq. (26) captures the basic properties of the real flames, the global effects of the combustion on a gas flow will be accounted for. It is possible to briefly enumerate some of these fundamental properties. First of all, a correct flame velocity and flame thickness allow to properly estimate the scale of the vortices able to cross the flame front in combustion/turbulence studies and thus the flame wrinkling and turbulent velocity. It is also necessary to capture extinctions of the flame if the local dissipation rate increases. Eventually, ignition delay is also a fundamental parameter in some specific studies. However, single-step chemistry cannot characterize ignition delays, which are directly linked to the rate of creation of intermediate species.

The most basic model from global kinetics point of view is for non-premixed combustion. An infinitely fast reaction between fuel and oxidizer occurs because both of them react instantaneously as soon as they meet and the flame is therefore controlled by the species mixing. Only the heat release (first property) is captured by this model that is only valid for very high Damköhler numbers. However, even if its global properties and behavior are wrong, this instantaneous and simple method may be useful as a development procedure to test the ability of numerical and physical models to cope with the combustion heat release and the gas dilatation.

The next step to improve combustion chemistry is to introduce a single Arrhenius law that is commonly used to describe global kinetics. Its ability to capture most of the above properties (flame velocity, extinction phenomena...) has already been proved. However, problems appear when realistic stoichiometric coefficients and non-stoichiometric (or partially premixed) combustion are concerned, which is generally the case with spray combustion. As summarized by Poinsot and Veynante [9], asymptotic and numerical estimations of the flame speed as a function of the equivalence ratio (Φ) provide good estimates on the lean side ($\Phi < 1$) but fail on the rich side ($\Phi > 1$). In this last case, a constant growth of the velocity may be observed even for equivalence ratios greater than unity whereas it should reach a maximum value in the vicinity of $\Phi = 1$. This problem is linked to the pre-exponential function. To overcome this issue, which is fundamental for two-phase flows modeling, a pre-exponential correction for the Arrhenius law has to be prescribed [43]. By doing so, a significant number of fundamental properties and phenomena resulting from the combustion are characterized by a single-step kinetics. This pre-exponential correction of the Arrhenius law has been used in the present paper excepted for the section (4.5) for which a skeletal mechanism is considered.

3.6 Flame index

Previous sections were dedicated to numerical modeling description used in DNS-DPS. In order to analyze combustion regimes encountered in DNS-DPS, a specific tool needs to be defined. For this purpose, to differentiate the heat release due to non-premixed combustion from the one due to premixed combustion, Takeno *et al.* [44] proposed a

flame index based on the scalar product of the gradients of the fuel and oxidizer mixture fraction fields.

$$G_{FO} = \nabla Y_F . \nabla Y_O \tag{27}$$

In diffusion flames, gradients are facing each other and the index is negative. On the other hand, it is positive when burning in premixed regime. From this definition, a normalized index ξ_P [45] may be defined as follows:

$$\xi_P = \frac{1}{2}\left(1 + \frac{G_{FO}}{|G_{FO}|}\right) \tag{28}$$

with $\xi_P = 1$ in premixed mixtures and $\xi_P = 0$ for diffusion regimes. Then global heat release due to premixed combustion may be determined by the following relation:

$$\dot{\omega}_{prem} = \frac{\int \xi_P \dot{\omega} dv}{\int \dot{\omega} dv} \tag{29}$$

Similarly, the non-premixed heat release is:

$$\dot{\omega}_{diff} = \frac{\int (1 - \xi_P) \dot{\omega} dv}{\int \dot{\omega} dv} \tag{30}$$

where dv is an elementary volume and $\dot{\omega}$ is the global heat release of the reaction.

3.7 Droplet preferential segregation

When combustion takes place, fuel/air mixture is the key parameter defining flame structure and combustion regime. This mixture is directly linked to the local liquid density. To study the preferential concentration of discrete particles in turbulent flows, several approaches exist, see for instance references [14, 16, 46, 47, 48]. If a statistically homogenously distributed spray is randomly injected, i.e. if there is no preferential segregation, the distribution of the number of particles per control volume (CV) of a given size must follow a binomial distribution, which may be approximated by a Poisson distribution in our configurations. Hence, the study of the preferential concentration is usually based [46] on the difference between the actual segregated distribution and the Poisson distribution. It is characterized by:

$$\Sigma = (\sigma - \sqrt{\lambda})/\lambda \tag{31}$$

where λ is the average number of particles per cell and σ and $\sqrt{\lambda}$ are the standard deviations of the particle distribution and the Poisson distribution, respectively. For a given Lagrangian distribution of the particles, Σ strongly depends on the size of the considered CV. However, according to Fessler *et al.* [46], the length scale corresponding to the characteristic cluster size is equal to $\Delta_{\Sigma max}$, which is the size of the CV when Σ reaches a maximum value. In the present paper, the term *cluster* denotes a cloud of independent droplets in close proximity. It has been shown [49] that preferential segregation may also be characterized by the local Eulerian liquid density $\xi(\mathbf{x}, t)$ and its deviation ξ'. ξ corresponds to an instantaneous repartition of the liquid mass onto the Eulerian nodes with the method described above (see section 3.4). It appears that the length scale corresponding

to the most energetic mode of the fluctuations of ξ' is equal to $\Delta_{\Sigma max}$ that is obtained through a Lagrangian procedure. From both the numerical and the experimental point of views, droplet segregation mainly depends on their Stokes number (St is the ratio of the droplet kinetic time to a characteristic time of the turbulence). Segregation phenomena reach a maximum when the Stokes number, based on the Kolmogorov turbulent time scale, reaches unity (2 and Fig. 3).

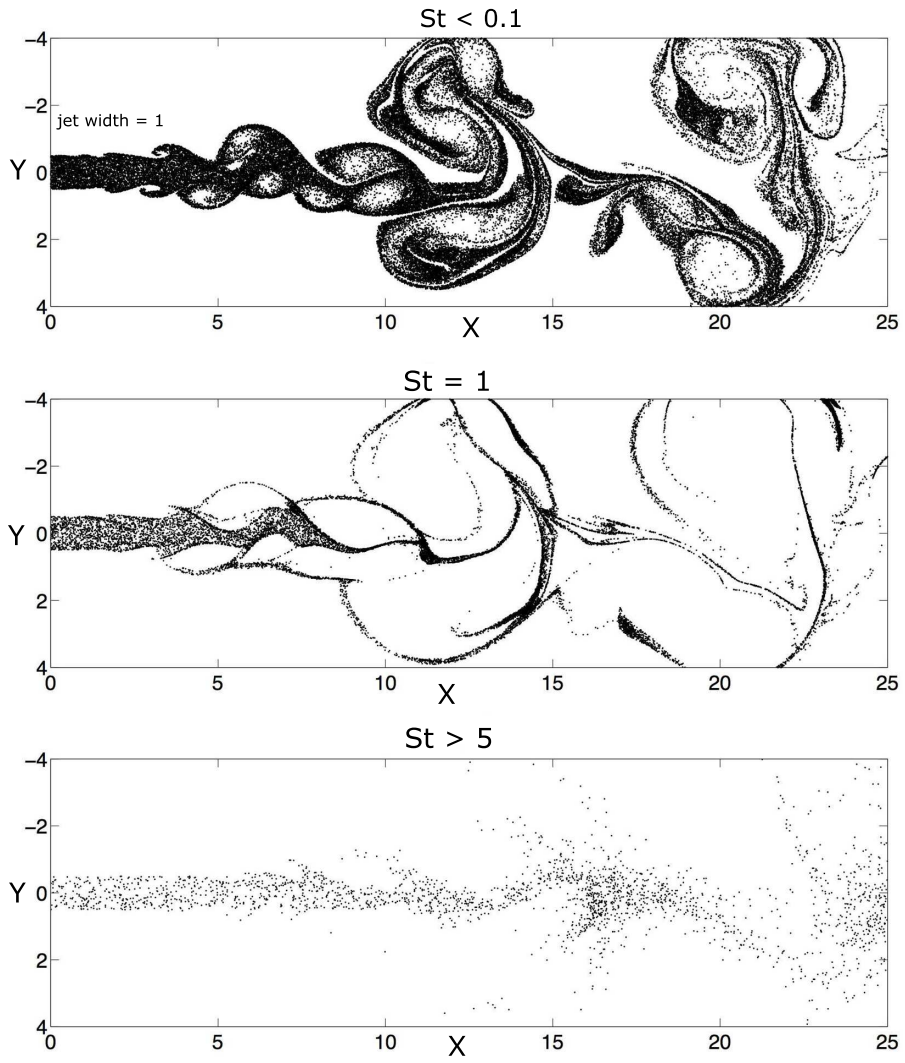

Figure 2: Example of droplet dispersion with respect to the droplet Stokes number in a turbulent jet.

From a phenomenological point of view, the evolution of the size of the clusters results from the competition between three physical phenomena: the ejection of the droplets from the vortex cores by the turbulence, the turbulent micro-mixing (prevalent when $St < 1$) and the ballistic effects (prevalent when $St > 1$). Indeed, droplets tend to be ejected from the turbulent structures to form clusters concentrated in low vorticity areas. However, for droplets with a small Stokes number, turbulent micro-mixing counteracts the segregation process and 'diffuse' clouds are obtained (as seen in Fig. 2): the lighter the droplets, the

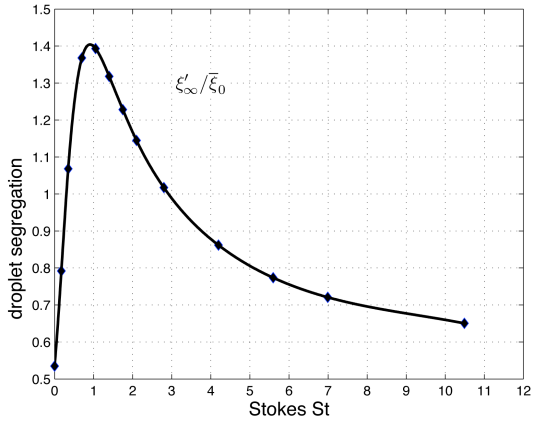

Figure 3: Droplet segregation level with respect to the Stokes number [49], $\xi'/\overline{\xi}_0$ is the liquid density deviation normalized by the mean liquid density.

more effective the mixing and the larger the characteristic size of the clusters. When $St = 1$, an optimal segregation is obtained because micro-mixing is weak and the droplets are not heavy enough to leave low vorticity areas where they are trapped. However, as soon as inertia is prevalent ($St > 1$) the particles are able to cross turbulent structures no matter what their vorticity is and the characteristic size of the clusters increases again.

4 EXAMPLES OF APPLICATIONS OF REACTIVE DNS-DPS

4.1 Introduction

It is usually stated that there is a missing link between DNS-DPS and experimental results. Direct numerical simulation implies a minimal number of nodes $n > Re_t^{3/4}$ along each direction of the domain to characterize all scales of turbulence. Today, capabilities of supercomputers are too low to simulate domain bigger than a few cm^3. Moreover, even if we could simulate grids with billions of nodes, there would be a lack of storage facilities that would impose to preselect the data to store for further analyses. The main advantage of DNS (access to all data at any time) would be seriously restricted. Consequently, specifics of the DNS make comparison with experiment difficult even if DNS is a powerful tool to complement the experimental data.

Comparisons of DNS and experiment may be carried out following two ways. A first possibility is to consider a configuration where a scale similarity assumption may be done. The small DNS domain is then compared to the real size experiment. If all the characteristic scales of the flow are of the same order of magnitude, normalized experimental and DNS results should match. A second possibility is to consider a small experimental configuration and to perform a real size DNS. A low Mach number assumption is often necessary to have reasonable computational time. In this case, experimental configurations are those to be restricted but a qualitative (sometimes quantitative) comparison

between numerical and experimental results is possible.

Eventually, one must not forget that DNS-DPS describes all the properties of the flow and the multiple interactions between physical phenomena, as far as they have been introduced in the differential equations describing our system. When this condition is satisfied, DNS-DPS is a powerful tool to understand physics and to develop models for RANS or LES simulations.

In the following, some comparisons between DNS-DPS and experiments are presented. First, it is shown that even 1D simulations offer information allowing to understand experimentally-observed physical phenomena. Then, qualitative comparisons of premixed and non-premixed combustion regimes are shown as well as qualitative comparison between DNS-DPS and experiment for spray flame interactions with acoustic waves. The last example extends the DNS-DPS potential to the auto-ignition process by introducing skeletal chemical kinetics.

4.2 Laminar spray flame

Depending on the configuration of the studied system, combustion may take place either after the full evaporation of the liquid fuel or within the evaporating dispersed phase. In the first case, even if classic gaseous combustion models can be used, the mixture fraction topology issued from the spray evaporation is completely different from the one obtained with a gaseous fuel injection. As described in the previous section concerning spray preferential segregation, partially premixed areas appear and various flame structures may be generated depending on the droplet dynamics.

For purely gaseous flows, the definition of the equivalence ratio is straightforward. It is defined as the ratio of the actual fuel/air ratio to the stoichiometric one. Following the topology of the mixture fraction, it is thus possible to precisely anticipate combustion regimes and reaction rates based on the amount of fuel and oxidizer injected in the combustion chamber. In the framework of two-phase flow combustion, knowing the mass flow rates of liquid fuel and gaseous oxidizer in the chamber is not enough to determine the local effective equivalence ratio. After atomization, liquid fuel is embedded in the gaseous oxidizer and may cross various regions for which thermodynamics (mainly temperature and pressure) properties affect (1) the evaporation rate of the droplets and (2) the local mass fraction of oxidizer and thus the local equivalence ratio. Similar phenomena occur when a front flame is present. Heat transfers may lead to a local extinction of the flame. For example, among other phenomena, it appears that a stoichiometric injection of fuel and oxidizer may lead to non-stoichiometric flames.

When flames propagate in a mixture where evaporating droplets are still present, numerous complex interactions between combustion, droplet evaporation and turbulence occur. The spray locally modifies heat transfer, momentum, dissipation rate and, of course, the mixture fraction level. All these variables deeply affect the flame ignition and propagation but also the characteristic properties of the turbulence. It is then particularly difficult to isolate the elementary physical phenomena and to analyze the fundamental interactions. For example, it has been experimentally observed that combustion instabilities may occur (Fig. 4-(a)) when a laminar flame propagates even though the Lewis number is unity [50]. A similar purely gaseous flame would be stationary. Thanks to

DNS-DPS, it is possible to retrieve and analyze these instabilities.

DNS-DPS allows to highlight that spray combustion can occur following periodic pulsations leading to the fluctuation of the (laminar) flame velocity (Fig. 4-(b)). The basic physical pattern is the following: at first, evaporation begins while maximum reaction and evaporation rates are weak. As soon as vapor and oxidizer mixture reach an ideal state, a flame front strongly propagates and drives the evaporation front. However, the characteristic times of the flame are shorter than the evaporation delay. Therefore, the flame front quickly depletes the vapor so that extinction occurs. This process occurs with a period of 20 μs for the example plotted in Fig. 4-(b).

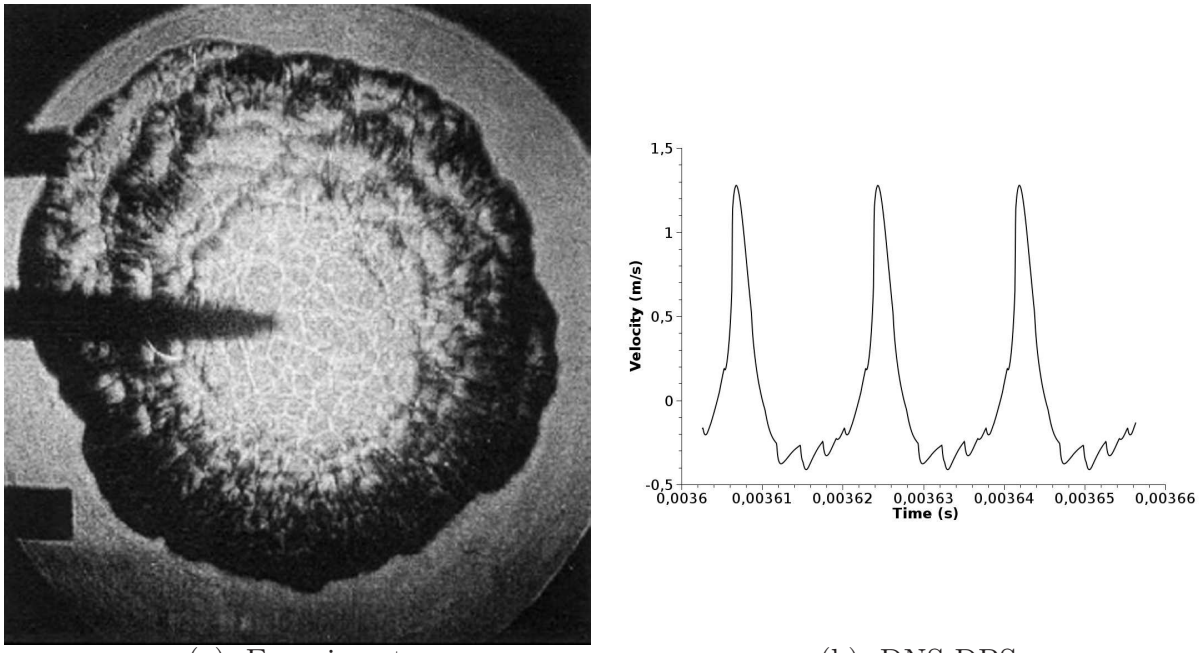

(a): Experiment (b): DNS-DPS

Figure 4: Apparition of spray flame instabilities for a unitary Lewis number. (a) Laminar expansion of a spray flame, experiments (flame front development) from Atzler *et al.* [50], instabilities are observed on the flame surface. (b) Simulation (DNS-DPS) of the propagation of a 1D spray flame. The relative flame velocity is represented. Instabilities appear because of the competition between the droplet evaporation time and the flame velocity.

This simple example shows the complexity of spray combustion. Indeed, many characteristic parameters are involved: the flame velocity, the flame thickness, the heat release, the droplet size, the droplet inter-space, the evaporation time... By only modifying one of these parameters, the flame dynamics may be dramatically changed.

4.3 Turbulent spray flames

As detailed in Reveillon and Vervisch [3], it is possible to classify spray flame morphology. Originally, the diagram (Fig. 5-(a)), developed by Chiu and coworkers [51, 52, 53, 33] consisted in the determination of the structure of flames propagating through a cloud

of droplets plunged in a preheated oxidizer. Spray combustion regimes were classified according to a group combustion number G defined by Candel *et al.* [54]: $G \approx 5N^{2/3}/S$. N is the total number of droplets in the cloud. The separation parameter $S = \delta_s/\delta_{r_f}$ is the ratio between δ_s, the mean droplet inter-space, and δ_{r_f}, the radius of a diffusion flame surrounding a single vaporizing drop in a quiescent oxidizer and having the mean properties of the spray (radius and evaporation time). When the separation number S decreases, there is a point where the flame topology evolves from individual droplet combustion to group combustion. For a given value of S, varying N, the number of drops in the liquid cloud, two major modes (Fig. 5-(a)) of spray combustion may be identified with respect to the group number G. In the first case, $G >> 1$, only an external layer of droplets evaporates and the resulting flame remains at a standoff distance from the spray boundary. At the other limit, $G << 1$, the droplets are sparse enough to allow the hot gases to reach the core of the spray. Consequently, evaporation and combustion processes take place around each individual droplet. Those conditions delineate the so-called "External" combustion regime expected for $G >> 1$, which is complemented by the "Internal" combustion regime, observed for $G << 1$ (Fig. 5-(a)).

Later on, Chang and Borghi [55, 56, 57, 58] added to the analysis the control parameters of the reaction zone itself, namely the characteristic flame time τ_f and its thickness δ_f. In addition, the mean evaporation delay τ_v was introduced. When $\tau_v << \tau_f$, the mixture may locally be premixed and a propagating premixed flame develops. If the evaporation time is large enough, for $\delta_f > \delta_s$, the collection of drops penetrates the reacting diffusive layers since the flame is broader than the mean droplet interspace δ_s. This situation should rapidly promote the thickening of the flame. Aside from these extreme cases, the separation number (S) should be introduced. After the propagation of a primary partially premixed front, some droplets may persist, leading to a secondary (or back-flame) reaction zone. The topology of this secondary combustion zone depends on the magnitude of S. For small values of S, the droplets are individually burning or are clustered in small groups surrounded by a flame. This is called the "Group" combustion regime. In complement, Borghi *et al.* have distinguished a "Percolation" combustion regime and a "Pocket" combustion regime subsequently appearing when the separation number S increases (Fig. 5-(b)).

Chiu *et al.* [33] and Borghi *et al.* [58] have defined these flame structures in the case of a quiescent spray without considering the global liquid fuel/air mass ratio. However, within a real spray combustion system, this key ratio is known to modify flame stability along with the overall properties of the combustion chamber. Changing it would affect the distribution of the local equivalence ratio of the gaseous mixture. Specifically, the topology of the primary and secondary reaction zones may vary a lot with this additional parameter. Cessou and Stepowski [59] have performed planar visualization of OH emissions in ethanol flames. As mentioned above, it is always difficult to compare DNS-DPS with experiments, because of numerous restrictions. However, the three major characteristic regimes found in the experiments are recovered in the DNS-DPS of turbulent spray flames (Fig. 5-(c)). They reflect the trends discussed above, spray-jet equivalence ratios above unity lead to rich partially premixed combustion associated to diffusion flame burning and to an "Open external" combustion regime displayed in Fig. 6-(a). Decreasing the spray-jet equivalence ratio within the flammability limits brings an "Hybrid" regime (Fig. 6-(b)). The last

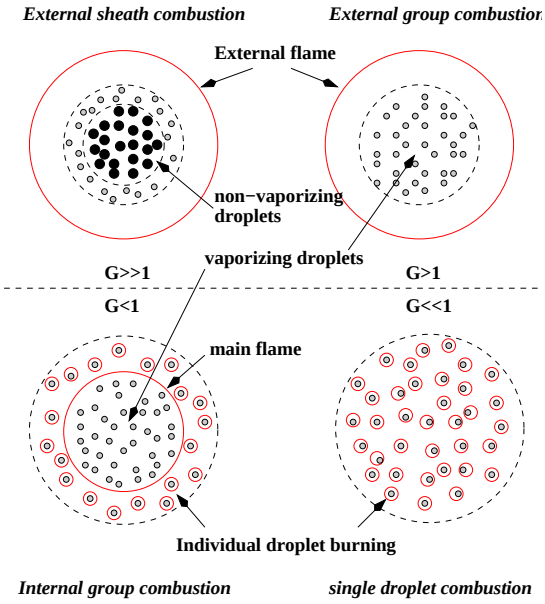

(a): Droplet Clouds

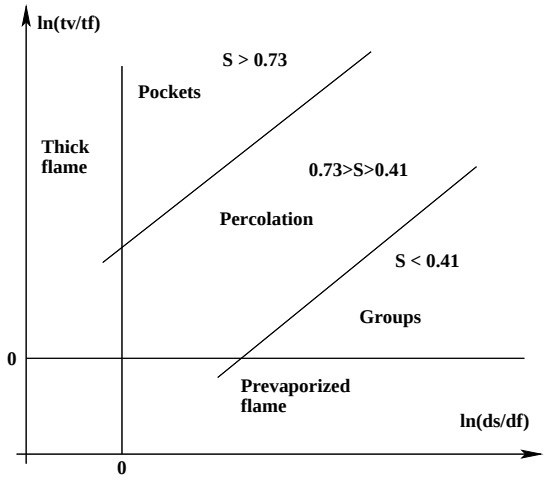

(b): Laminar flame

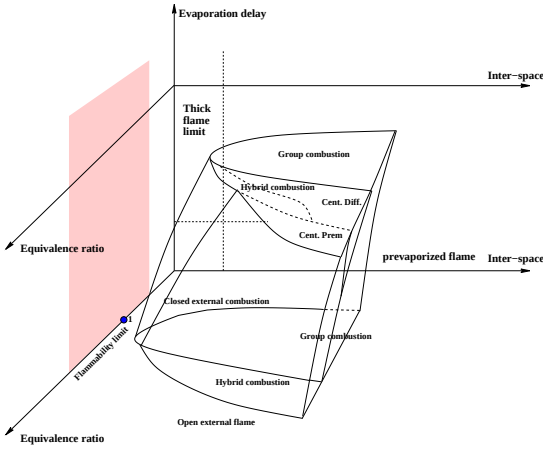

(c): Turbulent flame

Figure 5: Spray combustion diagrams development.

case has motivated many discussions on spray-flame topologies, since it is not obvious to determine the exact flame structure from the OH field showing very intricate radical layers (Fig. 6-(c)). The DNS-DPS having a burning mode featuring a central and an outer diffusion flame (characterized thanks to the flame index defined in section 3.6) may be compared to this intriguing planar visualization, even though it should be noticed that this comparison has been performed at a qualitative level only.

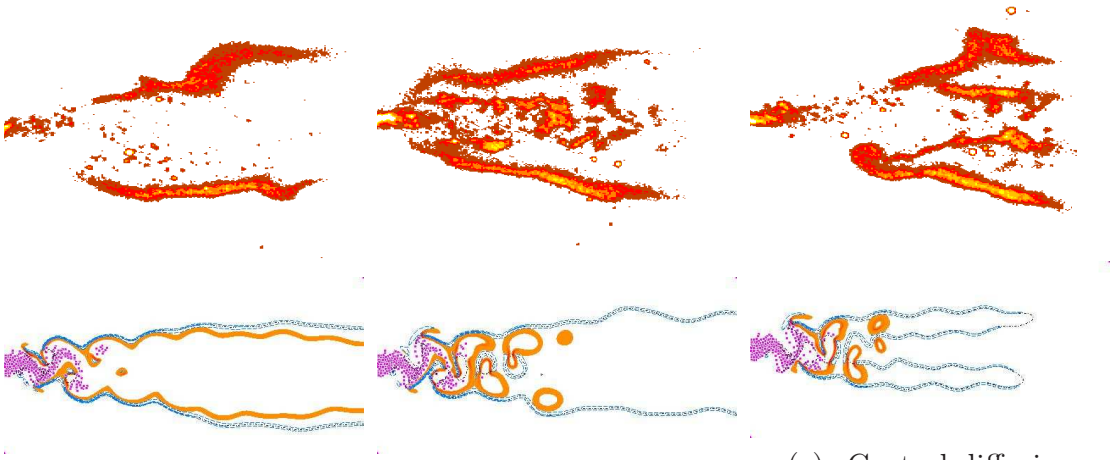

(a): Open external regime (b): Hybrid regime (c): Central diffusion flame

Figure 6: Qualitative comparisons of spray-jet flames. top line: Cessou and Stepowski [59] experimental measurement of planar visualization of OH emissions in ethanol flames. bottom line: DNS-DPS from Reveillon and Vervisch [3]. Orange lines correspond to premixed regime (Eq. (29)) whereas blue dashed-lines are diffusion reaction rates (Eq. (30)). Symbols represent droplets.

4.4 Acoustic modulation and spray flames

Combustion instabilities are observed in numerous industrial systems and more particularly in aeronautical engines: turbojets, ramjets, rocket motors... They create many undesirable effects such as an increase of wall heat fluxes, flame extinction and flashback or strong vibrations of the mechanical structure, which can lead to its destruction. In spite of many research tasks dedicated to this topic, these instabilities are difficult, if not impossible, to predict.

The objective of the configuration shown in Fig. 7 is twofold: first, to demonstrate the capability of a DNS-DPS solver to capture the complex spray/flame/acoustic interactions and then, to focus on the influence of velocity modulations on reaction rate through an analysis of the transfer function. This configuration has already been detailed in Pera and Reveillon [60]. A classical Bunsen configuration has been selected and experimental comparisons were made possible thanks to the data of the EM2C laboratory, Ecole Centrale Paris.

N-heptane is considered for both gaseous and two-phase flow configurations. The burner injection radius is equal to $R_b = 7.5 \ \ mm$. The mean injection velocity is equal to $u_{z0} = 2 \ \ m/s$. It is approximately four times faster than the reference stoichiometric laminar flame velocity ($45 \ \ cm/s$). The amplitude of the added velocity fluctuations reaches 10 % of the mean flow velocity. The whole experimental setup is oriented from top to bottom so that the heaviest droplets fall into the flame instead of going back into the burner.

Two experimental configurations have been selected:

- The "GAS" configuration involves a purely gaseous flow and leads to a classical

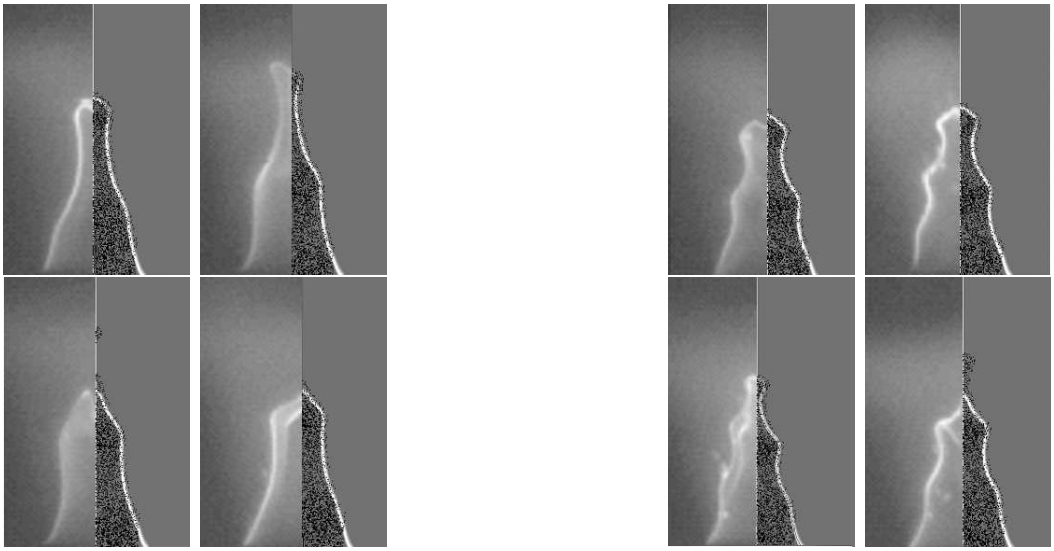

(a) - $\omega^*_{GAS} = 12$ (b) - $\omega^*_{GAS} = 23$

Figure 7: Qualitative comparison between experimental (cone left side) and numerical (cone right side) of a pulsating spray Bunsen flame (DRPE) for two acoustic modulations. The experimental flame front has been measured thanks to OH chemiluminescence whereas DNS-DPS one is plotted through the global reaction rate. On the cone right side, black points are Lagrangian droplets.

Bunsen flame with a stoichiometric mixture.

- The "DRPE" configuration is dedicated to two-phase flow combustion. N-heptane droplets are injected along with the main gaseous stream. To stabilize the conical flame near the burner lips, gaseous n-heptane is added in the main stream. A mass ratio of 1/4 of liquid fuel and 3/4 of gaseous fuel has been used to globally reach stoichiometry. Gaseous fuel has been obtained by slightly preheating a part of the liquid phase before the injection.

To characterise the response of the flame to the velocity modulation, the flame transfer function F_{tr} has to be defined. A very thin flame is considered. It undergoes the following modulation of the flow: $u_z(\mathbf{x}, t) = u_{z0}(\mathbf{x}) + u'_z(\mathbf{x}, t)$, where u_{z0} is the flow mean velocity and u'_z the velocity modulation which amplitude and frequency are A_u and ω, respectively. The flame transfer function F_{tr} is defined by the ratio of the relative fluctuation of the heat release amplitude $A_Q/\underline{Q}$ with the relative fluctuations of the velocity field amplitude A_u/u_{z0} :

$$F_{tr} = \frac{A_Q}{\underline{Q}} \frac{u_{z0}}{A_u} \tag{32}$$

where $\underline{Q}$ is the mean flame heat release and A_Q is the amplitude of the heat release fluctuations. More details may be found in [61, 62, 63].

A simple way to analyze flame interactions with a modulated acoustic field is to define a reduced frequency [62, 64] which main characteristics may be compared with the

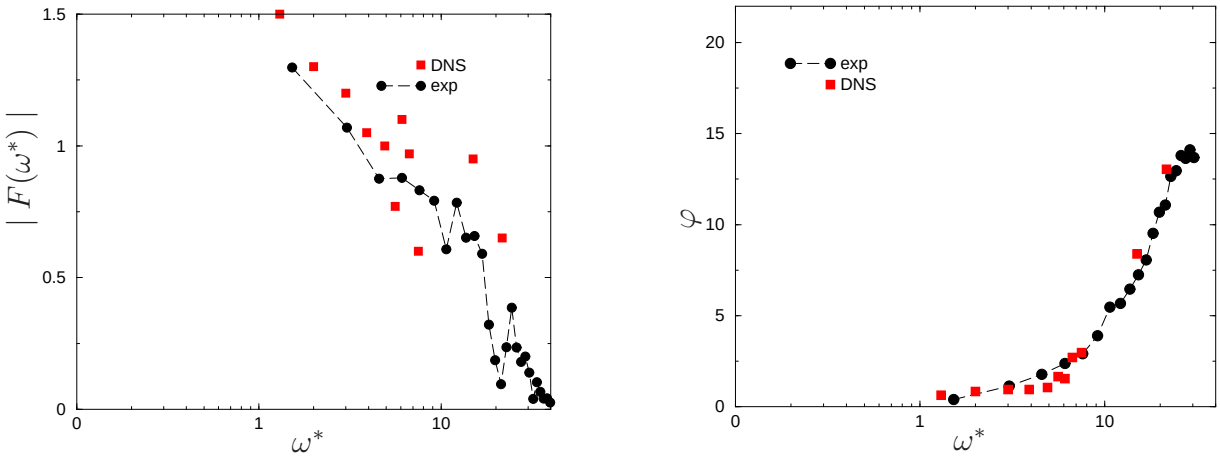

(a): Amplitude (b): Phase

Figure 8: Comparison between experimental results and numerical DNS-DPS simulation (a) amplitude and (b) phase transfer function (Eq. (32)) for two-phase flow Bunsen burner condition (DRPE).

stationary (no acoustic modulations) conical flame properties:

$$\omega^* = \frac{\omega R_b}{S_L^0 cos\alpha_0} \tag{33}$$

where ω is the effective pulsation, S_L^0 the reference stoichiometric planar flame velocity and α_0, the half-angle at the top of the cone.

4.4.1 Stationary flames

Qualitative comparisons of the experimental and numerical flame fronts are done for both GAS and DRPE configurations without any acoustic modulation. Thus a stationary cone is observed. The cone angle is well captured by DNS-DPS. Indeed, the cone height ratio of the DRPE flame with the GAS flame is $\frac{H_d}{H_g}|_{exp} = 0.88$ as measured experimentally. The corresponding ratio obtained with the DNS-DPS is slightly different ($\frac{H_d}{H_g}|_{DNS} = 0.85$) but still a good catch of the general decreasing behavior. Note that the 'stationary' experimental flame (no acoustic modulation) shows various perturbations because some clouds of droplets create disturbances of the flame front before burning outside the main cone. These disturbances are not reproduced by the DNS-DPS computations because of a controlled homogeneous injection of the droplets.

4.4.2 Flame response to velocity modulations

To study the flame response to acoustic modulations, a sinusoidal velocity signal has been prescribed at the burner exist to mimic the loudspeaker effects.

Effects of medium ($\omega^*_{GAS} \approx 12$) and high frequencies ($\omega^*_{GAS} \approx 23$) are shown in Fig. 7. These figures correspond to the DRPE case. The inlet modulation generates a propagating signal along the flame front from the base up to the top of the cone. From a general point

of view, the lower the frequency is, the longer the flame. When frequency increases, the flame front is more and more perturbed. In some cases, it is possible to observe the formation of a pocket of fresh gases at the top of the cone and, when the flame retracts itself, this pocket is drifted away in the burnt gases an disappears very quickly. Good agreements may be observed between simulation and experiment (Fig. 7).

The amplitude of the experimental transfer function is well captured by DNS-DPS (Fig. 8-(a)). From the phase point of view (Fig. 8-(b)), DNS-DPS is in very good agreement with the experimental results up to a reduced frequency equal to 30.

These successful qualitative comparisons between DNS-DPS and experiments allowed us to validate the capability of the DNS-DPS to capture the physical phenomena embedded in the triple interactions: spray/combustion/acoustic modulation.

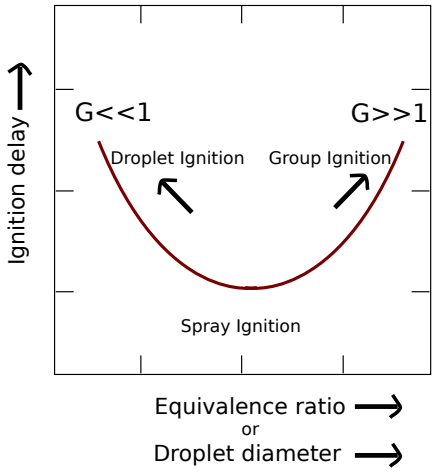

Figure 9: Qualitative description of the three auto-ignition modes in sprays, from Aggarwal [65].

4.5 Spray auto-ignition

In the context of direct injection car engines, detailed understanding of the basic physical and chemical phenomena involved in two-phase flow auto-ignition is crucial. However, numerical [23, 66, 67] and experimental [68, 69] works on two-phase flow auto-ignition are still scarce and only a few general trends are known. It appears that the reactivity of two-phase flow mixtures is controlled by two competing processes [70]: heat transfers due to the evaporation of the liquid fuel and heat release due to early combustion reactions. The influence of temperature and pressure is discussed in Aggarwal [65] along with the fact that droplet size and ignition delays are strongly related. As summarized by the sketch in Fig. 9 issued from the review paper of Aggarwal [65], the droplet size largely influences the auto-ignition delay in relation with the available gaseous equivalence ratio. From a qualitative point of view, there are three dominant spray ignition modes and corresponding ignition delays. First, similarly to the combustion regimes previously mentioned, ignition can occur either individually for each droplet ($G << 1$), or around clouds of droplets ($G >> 1$) if droplets are too close to each other to allow for diffusion of heat inside the

cloud. A third mode, the *Spray Ignition* mode, considers a global ignition of the spray for droplets close to each other but surrounded by a hot atmosphere.

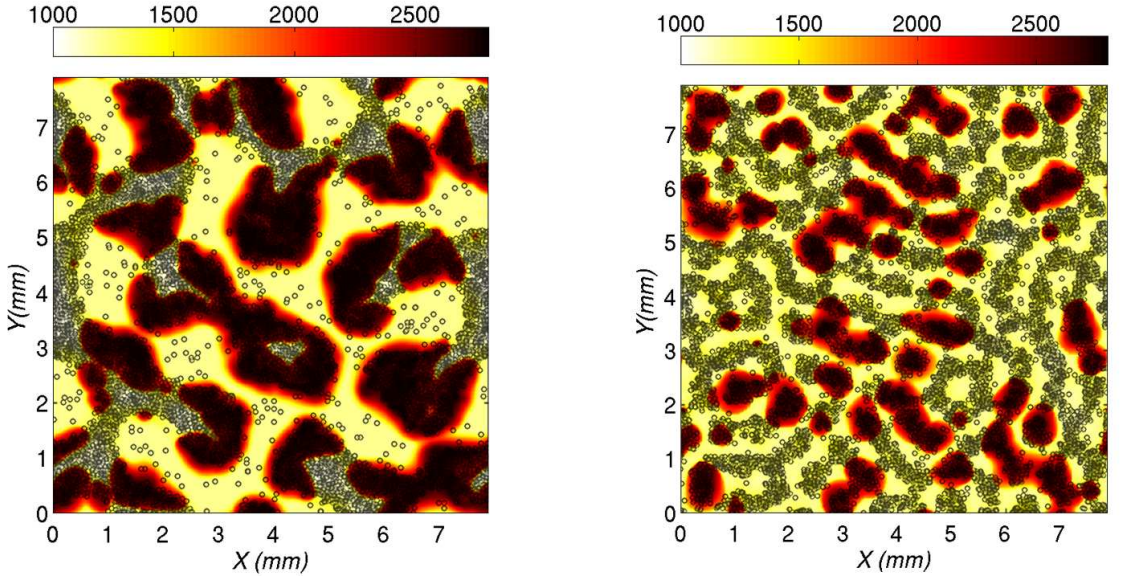

(a): Characteristic droplet cloud size: 2 mm

(b): Characteristic droplet cloud size: 0.65 mm

Figure 10: Example of the auto-ignition of sprays with various characteristic sizes of the clouds of droplets (a) - 2 mm and (b) - 0.65 mm. Represented: Temperature (color) and initial droplet position (symbols). The initial temperature of the carrier phase is 1200 K. Fields are presented for time around 1.5 ms.

Most of the auto-ignition studies are based on non-dimensional reactors. They generally focus on the links between heat transfers (leading to a gaseous temperature decrease due to the droplet evaporation) and chemical kinetics. They offer major insights into the influence of a liquid phase onto the ignition properties but they cannot characterize any geometrical aspect of the spray dispersion (no spatial information). In practical systems, preferential segregation of droplets (see section 3.7) very early appears because of the strong turbulent mixing [71]. It leads to the formation of non-homogeneous pockets of fuel vapor that cannot be characterized by non-dimensional approaches though there is a direct influence on combustion regimes and model performances. The objective of the present example is to use DNS-DPS to extend homogeneous reactors studies to a multiple cloud system, the size and droplet density of which are prescribed. It allows accounting for the geometrical aspect of the spray in addition to the fundamental thermodynamical properties. The new geometry is bi-dimensional in order to take into account the preferential segregation of droplets while maintaining reasonable CPU times. The segregation is characterized by the spray density variance and the characteristic size of the clouds (or clusters) of droplets. The DNS-DPS solver is coupled with the Chemkin solver using the n-heptane kinetics of Patel *et al.* [40]. This skeletal mechanism involves 29 species and 52 reactions. It has already been successfully compared to other reference complex chemistries [40]. Of course, three-dimensional computations would be better. However, computational costs would be skyrocketing to simulate a sufficiently large configuration

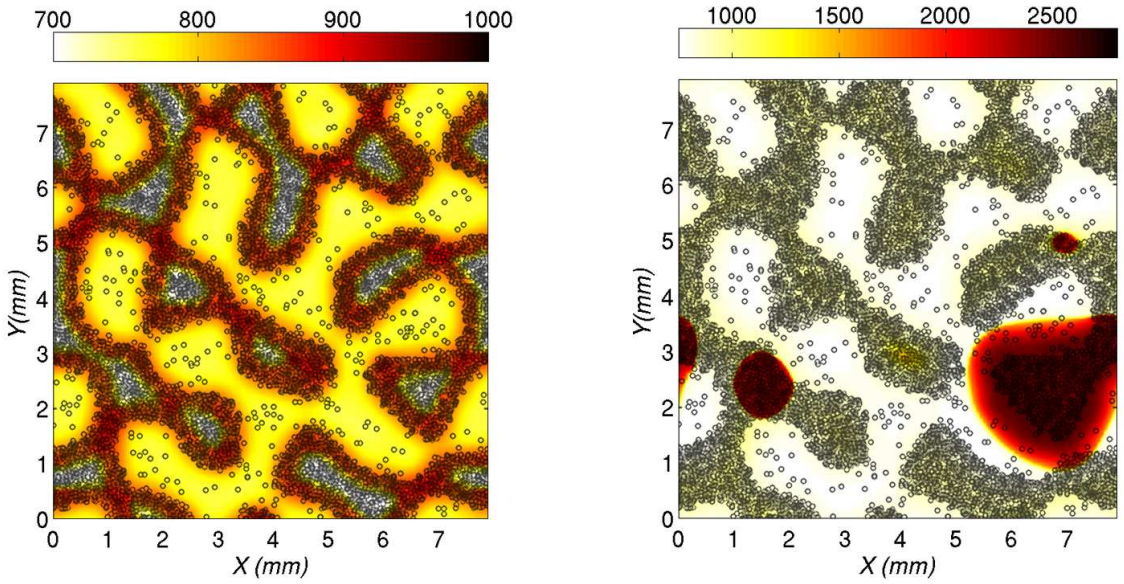

(a): Cool flame (b): Full ignition

Figure 11: Example of the auto-ignition of a highly segregated spray embedded in a gaseous oxidizer. Represented : Temperature (color) and initial droplet position (symbols). The initial temperature of the carrier phase is 750 K. At first, a slightly exothermic reaction heats the gas up to 1000 K (a - Cool flame - 8 ms). Then auto-ignition occurs at the droplet cloud's boundaries before reaching its core (b - Full ignition - 9.3 ms). Note the difference in the temperature scale for pictures (a) and (b).

to carry out accurate statistics. It remains a technical challenge that still needs to be addressed.

This work is based on the pioneering studies of Wang and Rutland [23, 24] who have used a similar DNS-DPS formalism, with skeletal chemistry mechanism for n-heptane. They have analyzed high temperature chemistry of two-phase flows in two-dimensional geometries. We presently extended their configuration by prescribing various sizes of droplet clouds and additionally analyzing low temperature chemistry as well. A homogeneous and isotropic turbulent configuration is proposed: droplet clouds made of a monodispersed spray with a droplet diameter of 7 μm have been generated thanks to a spectral procedure [72] to control any scale of the flow. The spray is embedded in an initially quiescent preheated atmosphere. Two initial temperature levels T_0 have been considered: 750 K and 1200 K and two characteristic sizes of droplet clouds are presented: 2 mm and 0.65 mm. The domain size is a square box with a side length of 8 mm (Figs. 10 and 11). Despite the initially quiescent atmosphere, gas dilatation generates convective streams as soon as ignition occurs.

Figure 10 presents the auto-ignition of the two sprays in a hot atmosphere ($T_0 = 1200\ K$) during reaction runaway. Although droplet cluster size is different, Fig. 12 shows that the characteristic size of the droplet clouds does not largely modify the ignition delay in such a hot atmosphere. The reaction runaway is around 1.5 ms for both configurations (Fig. 12). The dotted and dashed lines show at first a decrease in the temperature that is due to the heat consumption necessary to evaporate the n-heptane droplets. Once mixing

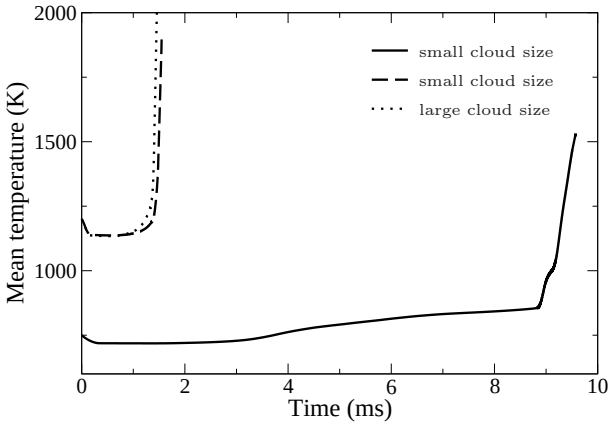

Figure 12: Evolution of average gas temperature for three initial conditions: two initial gas temperatures (750 K and 1200 K) and two characteristic sizes of droplet clouds (2 mm and 0.65 mm).

leads to appropriate gaseous fuel/air ratios, auto-ignition spots appear and grow (Fig. 10). Generally, ignition takes place at the border of droplet clouds before propagating into the cloud. This behavior is confirmed by the experimental work of Baritaud *et al.* [73] who have simultaneously presented spray liquid phase and auto-ignition spot location in a direct injection Diesel engine. For each engine cycle, Baritaud *et al.* [73] have observed self-ignition at the tip of the jet spray that can be considered as a cloud border in our configuration.

If the initial carrier gas temperature is diminished down to 750 K, auto-ignition follows a very different path. At first, it is possible to observe, in Fig. 12 (from the beginning to around 0.4 ms), a diminution of the temperature because of the evaporation process. Then, two successive cool flames with very different characteristic delays appear at 3 ms and later on at 8.8 ms. Cool flames are a direct consequence of intermediary exothermic reactions that occur before the full runaway. The first cool flame lasts more than 4 ms and may be visualized in Fig. 11, left picture. The temperature reaches a maximum of 1000 K at the border of the clusters whereas the core is still cold. The second cool flame is very quick (less than 0.2 ms) and is quickly overidden by the full auto-ignition process. In this case, the n-heptane chemistry is first favourable to auto-ignition of relatively lean mixtures that conversely lie within a relatively high temperature (because temperature decrease due to evaporation is less important where few liquid fuel is evaporated, *i.e.* at the cluster border). As a result, the cluster border first auto-ignites but in a cool flame regime that heats up the relatively rich central mixture. The heating-up can be sufficient to induce a direct main auto-ignition in the core of the droplet cloud.

This last example shows again the capability of DNS-DPS to analyze physical phenomena encountered in two-phase flow combustion. Of course, there are several limitations and constraints for these calculations but it may be a way to complement experimental works with precious information.

5 CONCLUSIONS

Through some examples, this paper illustrates the potential of the DNS to help to understand the reactive multiphase flows from preferential segregation distribution of the droplets to their effect on the auto-ignition process. In the context of reactive multiphase flows, intricate couplings often take place involving turbulent spray dispersion, mixing effects leading to specific mixture distribution and, of course, joined interactions with combustion. Althouth DNS-DPS is restricted to basic academic configurations, the various examples selected in this paper have been accompanied, when possible, with qualitative comparisons with experimental observations, which is still a rare approach in the framework of DNS. Good agreement between DNS-DPS and experiments demonstrates the potential of DNS-DPS to capture the physical phenomena while accessing to all the flow properties. As the comprehension of basic physics progresses, it allows the introduction into DNS-DPS of more detailed modeling concerning the liquid phase and chemistry reactions. While its range of applications is spreading, DNS-DPS becomes nowadays a powerful tool to go into details of basic physics as a complement of the experimental approaches.

References

[1] F. Mashayek. Direct numerical simulations of evaporating droplet dispersion in forced low mach number turbulence. *Int. J. Heat Mass transfer*, 41(17):2601–2617, 1998.

[2] R.S. Miller and J. Bellan. Direct numerical simulation of a confined three-dimensional gas mixing layer with one evaporating hydrocarbon-droplet-laden stream. *J. Fluid Mech.*, 384:293–338, 1999.

[3] J. Reveillon and L. Vervisch. Analysis of weakly turbulent diluted-spray flames and spray combustion regimes. *J. Fluid Mech.*, (537):317–347, 2005.

[4] S.A. Orszag and G.S. Patterson. Numerical simulation of three-dimensional homogeneous isotropic turbulence. *Phys. Rev. Lett.*, 28(2):76–79, Jan 1972.

[5] R.S. Rogallo. Numerical experiments in homogeneous turbulence. Technical report, NASA, 1981. Technical Memorandum No. 81315.

[6] S. Lee, K. Lele, and P. Moin. Numerical simulations of spatially evolving compressible turbulence. Technical report, Center for Turbulence Research Report, Stanford University, 1991.

[7] P. Givi. Model free simulations of turbulent reactive flows. *Prog. Energy Combust. Sci.*, 15:1–107, 1989.

[8] T. Poinsot, S. Candel, and A. Trouvé. Direct numerical simulation of premixed turbulent combustion. *Prog. Energy Combust. Sci.*, 12:531–576, 1996.

[9] T. Poinsot and D. Veynante. *Theoretical and Numerical Combustion, second edition.* Edwards, 2005.

[10] T. Poinsot and D. Veynante. *Theoretical and Numerical Combustion*. Edwards, 2001.

[11] C. Pantano, S. Sarkar, and F.A. Williams. Mixing of a conserved scalar in a turbulent reacting shear layer. *J. Fluid Mech.*, 481:291–328, 2003.

[12] J.J. Riley and Jr G.S. Patterson. Diffusion experiments with numerically integrated isotropic turbulence. *Phys. Fluids*, 17:292–297, 1974.

[13] M. Samimy and S.K. Lele. Motion of particles with inertia in a compressible free shear layer. *Phys. Fluids*, 8(3):1915–1923, 1991.

[14] K.D. Squires and J.K. Eaton. Preferential concentration of particles by turbulence. *Phys. Fluids*, 3(5):1169–1178, 1991.

[15] S. Elgobashi and G.C. Truesdell. Direct numerical simulation of particle dispersion in a decaying isotropic turbulence. *J. Fluid Mech.*, 242:655–700, 1992.

[16] L.P. Wang and M.R. Maxey. Settling velocity and concentration distribution of heavy particles in homogeneous isotropic turbulence. *J. Fluid Mech.*, 256:27–68, 1993.

[17] W. Ling, J.N. Chung, T.R. Troutt, and C.T Crowe. Direct numerical simulation of a three-dimensional temporal mixing layer with particle dispersion. *J. Fluid Mech.*, (358):61–85, 1998.

[18] F. Mashayek, F.A. Jaberi, R.S. Miller, and P. Givi. Dispersion and polydispersity of droplets in stationary isotropic turbulence. *Int. J. Multiphase Flow*, 23(2):337–355, 1997.

[19] J. Reveillon, K.N.C. Bray, and L. Vervisch. Dns study of spray vaporization and turbulent micro-mixing. In *AIAA 98-1028*, 36th Aerospace Sciences Meeting and Exhibit, January 12-15, Reno NV, January 1998.

[20] R.S. Miller and J. Bellan. Direct numerical simulation and subgrid analysis of a transitional droplet laden mixing layer. *Phys. Fluid*, 12(3):650–671, 2000.

[21] D.L. Marchisio and R.O. Fox, editors. *Multiphase reacting flows: modelling and simulation*. Springer, 2007.

[22] J.H. Chen, E.R. Hawkes, R. Sankaran, S.D. Mason, and H.G. Im. Direct numerical simulation of ignition front propagation in a constant volume with temperature inhomogeneities i. fundamental analysis and diagnostics. *Combust. Flame*, 145(1-2):128–144, 2006.

[23] Y. Wang and C.J. Rutland. Effects of temperature and equivalence ratio on the ignition of n-heptane fuel spray in turbulent flow. *Proc. Combust. Inst.*, 30:893–900, 2005.

[24] Y. Wang and C.J. Rutland. Direct numerical simulation of ignition in turbulent n-heptane liquid-fuel spray jets. *Combust. Flame*, 149:353–365, 2007.

[25] B. Lafaurie, C. Nardone, R. Scardovelli, S. Zaleski, and G. Zanetti. *Modelling merging and fragmentation in multiphase flows with SURFER*, volume 113. 1994.

[26] S. Tanguy and A. Berlemont. Application of a level set method for simulation of droplet collisions. *Int. J. Multiphase Flow*, 31(9):1015–1035, 2005.

[27] S. Tanguy, T. Menard, and A. Berlemont. A level set method for vaporizing two-phase flows. *J. Comp. Phys.*, 221:837–853, 2007.

[28] S.K. Lele. Compact finite difference schemes with spectral like resolution. *J. Comput. Phys.*, (103):16–42, 1992.

[29] A.A. Wray. Minimal storage time-advancement schemes for spectral methods. Technical report, Center for Turbulence Research Report, Stanford University, 1990.

[30] M.W. Reeks. On a kinetic equation for the transport of particles in turbulent flows. *Phys. Fluids*, 3(3):446–456, 1991.

[31] W.A. Sirignano. Fuel droplet vaporization and spray combustion theory. *Prog. Energy Combust. Sci.*, 8:291–322, 1983.

[32] K.K. Kuo, editor. *Principles of combustion*. John Wiley and sons, 1986.

[33] H.H. Chiu, H.Y. Kim, and E.J. Croke. Internal group combustion of liquid droplets. In The combustion institute, editor, *Proceedings of the nineteenth Symposium (International) on combustion*, 1982.

[34] C.T. Crowe, M.P. Sharma, and D.E. Stock. The particle-source in cell (psi cell) model for gas droplet flows. *J. Fluids Engineering*, pages 325–332, June 1977.

[35] F. Mashayek. Numerical investigation of reacting droplets in homogeneous shear turbulence. *J. Fluid Mech.*, 405:1–36, 2000.

[36] F. Lacas and X. Calimez. Numerical simulation of simultaneous breakup and ignition of droplets. *Proc. Combust. Inst.*, 28:943–951, 2000.

[37] C. Crowe, M. Sommerfeld, and Y. Tsuji, editors. *Multiphase flows with droplets and particles*. CRC Press, 1998.

[38] Y. Wang and C.J. Rutland. Effects of temperature and equivalence ratio on the ignition of n-heptane fuel droplets in turbulent flows. *Proc. Combust. Inst.*, 30, 2005.

[39] P. Schroll, A.P. Wandel, R.S. Cant, and E. Mastorakos. Direct numerical simulations of autoignition in turbulent two-phase flows. *Proc. Combust. Inst.*, 32(2):2275 – 2282, 2009.

[40] A. Patel, S.C. Kong, and R.D. Reitz. Development and validation of a reduced reaction mechanism for HCCI engine simulations. *SAE Paper 2004-01-0558*, 2004.

[41] D.G. Goodwin. An open source, extensible software suite for cvd process simulation. In *Proceedings of CVD XVI and EuroCVD Fourteen*. Electrochemical Society, 155–162, 2003.

[42] R.J. Kee, F.M. Rupley, J.A. Miller, M.E. Coltrin, J.F. Grcar, E. Meeks, H.K. Moffat, A.E. Lutz, G. Dixon-Lewis, M.D. Smooke, J. Warnatz, G.H. Evans, R.S. Larson, R.E. Mitchell, L.R. Petzold, W.C. Reynolds, M. Caracotsios, W.E. Stewart, P. Glarborg, C. Wang, C. L. McLellan, O. Adigun, W.G. Houf, C.P. Chou, S.F. Miller, P. Ho, P.D. Young, D.J. Young, D.W. Hodgson, M.V. Petrova, and K.V. Puduppakkam. Chemkin release 4.1. Technical report, Reaction Design Report - San Diego, 2006.

[43] J. Reveillon. *Direct numerical simulation of sprays: turbulent dispersion, evaporation and combustion*. In Marchisio and Fox [21], 2007.

[44] H. Yamashita, M. Shimada, and T. Takeno. A numerical study on flame stability at the transition point of jet diffusion flames. *Proc. Combust. Inst*, 26:27–34, 1996.

[45] V. Favier and L. Vervisch. Edge flames and partially premixed combustion in diffusion flame quenching. *Combust. Flame*, 125(1-2):788–803, 2001.

[46] J.R. Fessler, J.D. Kulick, and J.K. Eaton. Preferential concentration of heavy particles in turbulent channel flow. *Phys. Fluids*, (6):3742–3749, 1994.

[47] O. Simonin, P. Fevrier, and J. Laviéville. On the spatial distribution of heavy-particle velocities in turbulent flow: from continuous field to particulate chaos. *J. of Turbulence*, 118:97–118, 1993.

[48] A. Aliseda, A. Cartellier, F. Hainaux, and J.C. Lasheras. Effect of preferential concentration on the settling velocity of heavy particles in homogeneous isotropic turbulence. *J. Fluid Mech.*, 468:77–105, 2002.

[49] J. Reveillon and F.X. Demoulin. Effects of the preferential segregation of droplets on evaporation and turbulent mixing. *J. Fluid Mech.*, 583:273–302, 2007.

[50] F. Atzler, F.X. Demoulin, M. Lawes, Y. Lee, and N. Marquez. Burning rates and flame oscillations in globally homogeneous two-phase mixtures (flame speed oscillations in droplet cloud flames). *Combust. Sci. Technol.*, 178:2177–2198, 2006.

[51] T. Suzuki and H.H. Chiu. Multi droplet combustion on liquid propellants. In *Proceedings of the Ninth International Symposium on Space and Technology and Science*, pages 145–154, Tokyo, Japan, 1971. AGNE.

[52] H.H. Chiu and T.M. Liu. Group combustion of liquid droplets. *Combust. Sci. Technol.*, 17:127–131, 1977.

[53] H.H. Chiu and E. J. Croke. Group combustion of liquid fuel sprays. Technical report, Energy Technology Lab Report 81-2, Univ. of Illinois at Chicago, 1981.

[54] S. Candel, F. Lacas, N. Darabiha, and C. Rolon. Group combustion in spray flames. *Multiphase Sci. Tech.*, 11:1–18, 1999.

[55] S.H. Chang, editor. *Transport Phenomena in combustion*. Taylor and Francis, 1996.

[56] R. Borghi. *The links between turbulent combustion and spray combustion and their modelling*, pages 1–18. In Chang [55], 1996.

[57] R. Borghi. Background on droplets and sprays. In *Combustion and turbulence in two-phase flows, Lecture series 1996-02*. Von Karman Institute for Fluid Dynamics, 1996.

[58] R. Borghi and M. Champion, editors. *Modélisation et théorie des flammes*. Technip, 2000.

[59] A. Cessou and D. Stepowski. Planar laser induced fluorescence measurement of [oh] in the stabilization stage of a spray jet flame. *Combust. Sci. and Tech.*, 118(4-6):361–381, 1996.

[60] C. Pera and J. Reveillon. Dns study of the interactions between spray combustion and acoustic forcing. *Proceedings of the European Combustion Meeting*, page 1, 2005.

[61] C. Pera and J. Reveillon. Direct numerical simulation of spray flame / acoustic interactions. *Proc. Combust. Inst.*, 146(4):2283–2290, 2007.

[62] S. Ducruix, D. Durox, and S. Candel. Theoretical and experimental determinations of the transfer function of a laminar premixed flame. *Proc. Combust. Inst.*, 28:768–773, 2000.

[63] T. Schuller, S. Ducruix, D. Durox, and S. Candel. Modeling tools for the prediction of premixed flame transfert functions. *Proc. Combust. Inst.*, 29:107–113, 2002.

[64] S. Ducruix. *Dynamique des interactions Acoustique - combustion*. PhD thesis, Ecole Centrale Paris, 1999.

[65] S.K. Aggarwal. A review of spray ignition phenomena: present status and future research. *Prog Energy Combust. Sci.*, 24(6):565–600, 1998.

[66] R. Stauch, S. Lipp, and U. Maas. Detailed numerical simulations of the autoignition of single n-heptane droplets in air. *Combust. Flame*, 145:533–542, 2006.

[67] S. Sreedhara and Kang Y. Huh. Conditional statistics of nonreacting and reacting sprays in turbulent flows by direct numerical simulation. *Proceedings of the Combustion Institute*, 31(2):2335 – 2342, 2007.

[68] C. Wang, K. Shy, and L. Lieu. An experimental investigation on the ignition delay of fuel droplets. *Combust. Sci. Tech.*, 118:63–78, 1996.

[69] Q. Khan, S. Baek, and H. Ghassemi. On the autoignition and combustion characteristics of kerosene droplets at elevated pressure and temperature. *Combust. Sci. Tech.*, 179:2437–2451, 2007.

[70] V. Bykov, I. Goldfarb, V. Gol'dshtein, and J.B. Greenberg. Auto-ignition of a polydisperse fuel spray. *Proc. Combust. Inst*, 31(2):2257–2264, 2007.

[71] J. Reveillon and F.X. Demoulin. Effects of the preferential segregation of droplets on evaporation and turbulent mixing. *J. Fluid Mech.*, 583:273–302, 2007.

[72] J. Reveillon. Numerical procedures to generate and visualize flow fields from analytical or experimental statistics: turbulent velocity, fluctuating scalars and variable density sprays. *Journal of Flow Visualization and Image Processing*, 12(3):251–269, 2005.

[73] T.A. Baritaud, T.A. Heinze, and J.F. Le Coz. Spray and self-ignition visualization a di diesel engine. *SAE Technical Paper Series*, (940681), 1994.